The effect of autophagy and mitochondrial fission on Harderian gland is greater than apoptosis in male hamsters during different photoperiods

Zhe Wang
Qufu Normal University https://orcid.org/0000-0002-4950-9954
Jinhui Xu
Qufu Normal University
Junjie Mou
Qufu Normal University
Xiangyu Zhao
Qufu Normal University
Xiaocui Geng
Qufu Normal University
Ming Wu
Qufu Normal University
Huiliang Xue
Qufu Normal University
Lei Chen
Qufu Normal University
Laixiang Xu (xulx@qfnu.edu.cn)
https://orcid.org/0000-0001-9727-9754

Research

Keywords: photoperiod, Harderian gland, autophagy, apoptosis, mitochondrion

Posted Date: May 8th, 2020

DOI: https://doi.org/10.21203/rs.3.rs-26167/v1

The effect of autophagy and mitochondrial fission on Harderian gland is greater than apoptosis in male hamsters during different photoperiods

Zhe Wang[#1], Jin-Hui Xu[#1], Jun-Jie Mou[#1], Xiang-Yu Zhao[1], Xiao-Cui Geng[1,2], Ming Wu[1], Hui-Liang Xue[1], Lei-Chen[1], Lai-Xiang Xu[*1]

[1] College of Life Sciences, Qufu Normal University, 273165, Qufu, Shandong, China
[2] Yiheyuan school, 256100, Yiyuan, Shandong, China
# Zhe Wang, Jin-Hui Xu, and Jun-Jie Mou contributed equally to this work.

*** Correspondence:**
Lai-Xiang Xu
Email: xulx@qfnu.edu.cn

Abstract

Background: Photoperiod is one of the important factors of mammalian seasonal rhythm. As an important photosensitive organ in addition to the eyes and pinecones, Harderian gland (HG) may respond to seasonal light cycle changes. Here, we studied the morphological differences in the HG of male striped dwarf hamsters (*Cricetulus barabensis*), a small mammal with annual rhythm under different photoperiods (short photoperiod, SP; moderate photoperiod, MP; long photoperiod, LP), and further investigated the molecular mechanisms related to these morphological differences.

Results: Results showed that body weight, carcass weight, and HG weight were lower in the SP and LP groups than that in MP group. Terminal deoxynucleotidyl transferase biotin-dUTP nick end labeling (TUNEL) staining showed that random DNA fragmentation was observed in all three groups. The protein expression of bax/bcl2 and cytochrome C all have no significant difference between three groups, indicated that the level of apoptosis remained stable. Protein aggregation and mRNA expression of LC3 as well as the protein expression of LC3II/LC3I in the SP group were higher than that in the MP group. P62 protein aggregates and protein expression were lower in long photoperiod than other two groups. These results suggested that autophagy level was the lowest in MP group. The protein expression of ATP synthase and mitochondrial fission factor showed highest in MD group, while citrate synthase, dynamin-related protein1, and fission1 remain unchanged during three groups. These indicate that the mitochondrion fission and energy function are slightly reduced in SD and LD groups.

Conclusion: In summary, since the fact that there is no significant change in the level of apoptosis in HGs under different photoperiods, the significant up-regulation of autophagy level in the long and short photoperiod may be the main factor leading to the loss of HG weight as well as the reduced mitochondrial energy supply.

Keywords: photoperiod, Harderian gland, autophagy, apoptosis, mitochondrion

Introduction

Seasonal rhythm is an adaptive behavior of animals in temperate regions to seasonal changes and includes changes in development, reproduction, hair growth, and energy metabolism (1, 2). The HG, also known as the glandulae lacrimales accessoriae, covers the posterior part of two eyeballs and widely exists in mammals, birds, and reptiles (3, 4); the HG weight of jungle bush quail (*Perdicula asiatica*) reached the highest in May, which showed a significant seasonal variation rhythm (5). In addition, seasonal reproductive behavior in animals is known to be impacted by changes in temperature, humidity, food resources, and photoperiod (i.e., length of sunshine), with photoperiod being one of the most important factors (6). However, whether seasonal variation in the HG is related to photoperiod remains to be clarified.

The balance between apoptosis and autophagy is one of important mechanism for tissue weight maintenance (7). Study on rats showed that the long-term light note leads to the

increase of the level of apoptosis in HG (8, 9). Bax is one of the most important apoptotic molecules in mammals and is activated under high mitochondrial depolarization for translocation and insertion into the outer membrane of mitochondria via bax/bax-homo-oligomerization (10). This is followed rapidly by the formation and opening of a mitochondrial permeability transition pore (mPTP), through which cytochrome C (Cyto C), a mitochondrion-residing apoptogenic factor, is released into the cytosol, eventually leading to the cleavage of nuclear DNA and cell apoptosis (11, 12). At present, it is believed that DNA fragmentation detected by TUNEL staining is one of the most important indicators of increased apoptotic level (12). Furthermore, bcl2 inhibits apoptosis via suppression of bax/bax-homo-oligomerization (13, 14). Research has shown that high-intensity light stimulation or high-dose MT injection can lead to increased cell necrosis in the HG of female Syrian hamsters and male rats (15). As MT is usually positively correlated with the time of entry into darkness (3, 16, 17), short daylight exposure may increase the level of apoptosis in the HG.Quantitative analysis of apoptosis in the HG can help clarify the mechanisms related to the effects of photoperiodic changes on the morphology and function of the HG.

Autophagy is the phagocytosis of cytoplasmic proteins or organelles and their entrapment and degradation in vesicles (18, 19). As a key protein for autophagic lysosome formation, microtubule-associated protein 1 light chain (LC3-I) binds to the phosphatidylethanolamine (PE) complex to form LC3 II (20, 21), which is a marker protein of intracellular macrophages as well as changes in autophagy (21, 22). First discovered in 2013 (23), P62 is a transporter of degradable substances to autophagic lysosomes and is negatively related to autophagy levels in tissues (24). Quantitative analysis of LC3 and P62 proteins can indicate changes in autophagy level in the HG under different photoperiods. Melatonin can inhibit autophagy in the HG of female Syrian hamsters (25-27). To date, however, no research on the effects of photoperiod has been conducted in this field.

Changes in apoptotic and autophagic levels often involve mitochondrial function. Citrate synthase (CS) is a limiting enzyme of the tricarboxylic acid cycle (28, 29) and adenosine triphosphate (ATP) synthase is a rate-limiting enzyme of the ATP synthesis pathway (30). Thus, studies on CS and ATP can partly measure changes in mitochondrial function and energy supply of the HG during different photoperiods. Changes in mitochondrial function may involve mitochondrial fission. Dynamin-related protein 1 (DRP1) is a GTP-hydrolyzing mechanoenzyme that catalyzes mitochondrial fission in the cell, which drives division via GTP-dependent constriction (31, 32). The DRP1 receptor mitochondrial fission factor (Mff) is a major regulator of mitochondrial fission, with its overexpression resulting in increased fission (33). In contrast, DRP1 receptor fission 1 (FIS1) appears to recruit inactive forms of DRP1, and its overexpression inhibits mitochondrial fission (34, 35). Therefore, research on these three factors could highlight mitochondrial fission ability. However, there is a current lack of research on mitochondrial fission and the function of HG during different photoperiods.

Based on the above, the effects of photoperiod on the HG may be related to autophagy, apoptosis, and mitochondrial function. Current photoperiod studies in hamsters have mainly focused on changes in HG morphology (36-38). However, the mechanisms

involved in the morphological changes in the HG induced by different photoperiods, such as autophagy and apoptosis in small mammals during different photoperiods, remain poorly studied.The striped dwarf hamster (*Cricetulus barabensis*) is a small non-hibernating mammal widely distributed in the north temperate zone of Asia. In spring (March to April) and autumn (August to September), this hamster shows peak reproductive activities, while no reproductive activity occurs during the winter (December to January) (39, 40). Our previous research have shown significant seasonal changes in gene expression like *kiss1*and *gpr54* in the hypothalamus, regulation of immune function, and energy metabolism in these animal (41). Thus, research on photoperiodic changes in this species of hamster could provide further insights into seasonal rhythm changes in non-hibernating mammals.

Here, we studied the morphological changes, as well as the related mechanisms, in the HG under different photoperiods. We hypothesized that photoperiodic changes would affect the morphology of the HG and thus its function. We also hypothesized that changes in apoptotic and autophagic levels may be responsible for changes in the HG. To test these hypotheses, we studied the ultrastructural changes in the HG of hamsters under different daylight lengths. On this basis, the protein levels of apoptosis (bax, bcl2, and Cyto C) and autophagy (LC3 and P62)-related indicators were studied. We then quantified mitochondrial function (ATP synthase and CS) and fission level (DRP1, MFF, and FIS1).

Methods

Ethics Statement

All procedures followed the Laboratory Animal Guidelines for the Ethical Review of Animal Welfare (GB/T 35892-2018) and were approved by the Animal Care and Use Committee of Qufu Normal University (Permit Number: dwsc 2019010).

Animals and treatments

Striped dwarf hamsters were prepared as described previously in our laboratory (40, 41). Briefly, hamsters were captured from the cropland in Qufu region of Shandong Province, China (N35.78° E117.01°). This area belongs to the temperate continental monsoon climate, light, and temperature changes with the seasons obviously. The main vegetation are wheat, peanuts and corn.

Captured hamsters were acclimated in the animal feeding room and exposed to natural light for about 2 weeks. Hamsters were housed individually in cages (28 × 18 × 12 cm) at an ambient temperature of 22 ± 2 °C and relative humidity 55% ± 5%. Food (standard rat chow, Jinan Pengyue Experimental Animal Breeding Co., Ltd., China) and water was provided *ad libitum*.

Based on the body weight and degree of wear on upper molars, a total of 60 male adult hamsters (20–40 g) were randomly divided into three groups of 20 animals. Each group were placed into long photoperiod (16:8 h light／dark cycle; light from 04:00 to 20:00, LP), moderate photoperiod (12:12 h light／dark cycle; light from 06:00 to 18:00, MP) or short photoperiod (8:16 h light／dark cycle; light from 08:00 to 16:00, SP).

The hamsters for photoperiodic processing were placed in the cabin of biodiverse small animal feeding systems (NK, LP-30LED-8CTAR, Osaka, Japan). Temperature of cabin was 22 ± 2 °C, relative humidity was 55% ± 5% and light intensity was 150 ± 10 lx.

Photoperiodic processing lasted 8 weeks.

Sample preparation

At the end of the exposure, hamsters were sacrificed by CO_2 asphyxiation. The HGs were removed, with lengths and weights then recorded. The left HGs were immersed in glutaraldehyde-paraformaldehyde for transmission electron microscopy (TEM). The right HGs in each group were frozen in liquid nitrogen and stored in a refrigerator at −80 °C for subsequent Western blotting and immunofluorescence histochemical analyses. All procedures were carried out in accordance with approved guidelines.

Transmission electron microscopy (TEM)

The HGs were cut into blocks and immersed in 3% glutaraldehyde-paraformaldehyde. The blocks were then dehydrated with a graded series of ethanol and embedded in epoxy resin, with TEM then performed as described previously (42). A semithin section was applied to tissue samples, and after methylene blue staining (18), sections were adjusted under the microscope and sliced with an ultramicrotome (LKB-NOVA, USA). The ultrathin sections were double-stained with Reynolds' lead citrate and ethanolic uranyl acetate and then examined via TEM (JEOL, JEM-100SX, Japan). Images were processed with NIH Image software (Image-Pro Plus 6.0).

Fluorescence immunohistochemical analysis

Frozen 10-μm thick tissue cross-sections were cut from the mid-belly of the two lobes each sample at −20 °C with a cryostat (Leica, CM1950, Germany) and then stored at −80 °C for further staining. Randomly selected 10 sections of each lobe for the follow-up experiments. After 15 min of immersion in distilled water, the sections were stained in blocking solution (5% bovine serum albumin (BSA)) for 30 min at room temperature and then incubated with rabbit anti-LC3 (1:200, #ab48394, Abcam, Cambridge, UK) or rabbit anti-P62 (1:200, #18420, Proteintech, Wuhan, China) solution at 4 °C overnight. The sections were subsequently incubated with goat anti-rabbit Alexa Fluor 488 (1:200, #11034, Thermo Fisher Scientific, Rockford, IL, USA) at 37 °C for 2 h Images were visualized using a confocal laser scanning microscope (ZEISS, 880NLO, Germany) under krypton/argon laser illumination at 488 nm emitted light, with capture at an emitting fluorescence of 526 nm. Protein aggregations of LC3 and P62 were counted using a 100 μm × 100 μm area.

Terminal deoxynucleotidyl transferase biotin-dUTP nick end labeling (TUNEL) staining

DNA fragmentation induced by apoptosis was determined by double-labeled fluorometric TUNEL detection as described previously (10). The frozen sections were permeabilized with 0.2% Triton X-100 in 0.1% sodium citrate at 4 °C for 2 min and then incubated with an anti-laminin rabbit polyclonal antibody (1:500, #BA1761, Boster, Wuhan, China) at 4 °C overnight. After washing with PBS for 30 min, the sections were incubated with fluorochrome-conjugated secondary AF647 antibodies (1:200, #21245, Thermo Fisher Scientific) at room temperature for 2 h. Subsequently, TUNEL (#MK1023, Boster) reaction mixture was added at the recommended 1:9 ratio, and the sections were incubated for 60 min at 37 °C in a humidified chamber in the dark, as per the manufacturer's protocols. Finally, the sections were counterstained with DAPI (1:100, #D1306, Sigma-Aldrich, Saint Quentin Fallavier, France) at 37 °C for 30

min. Imaging was performed using a confocal laser scanning microscope with the same excitation and emission wavelengths as described above.

Western blotting

Western blotting was conducted as described previously (43). Protein was extracted from HGs and solubilized in sample buffer (100 mM Tris pH 6.8, 5% 2-β-mercaptoethanol, 5% glycerol, 4% SDS, and bromophenol blue), with protein extracts subsequently fractionated by SDS-PAGE using Laemmli gels and transferred to PVDF membranes (0.45-μm pore size) using a Bio-Rad semi-dry transfer apparatus. The blotted membranes were blocked with 1% BSA in Tris-buffered saline (TBS; 150 mM NaCl, 50 mM Tris-HCl, pH 7.5) and incubated with rabbit anti-bax (1:1000, #50599, Proteintech), rabbit anti-bcl2 (1:1000, #3498, Cell Signaling Technology CST, Danvers, MA, USA), rabbit anti-Cyto C (1:1000, #11940, CST), rabbit anti-LC3 (1:1000), rabbit anti-P62 (1:1000) and rabbit rabbit anti-ATP synthase (1:1000, #14676, Proteintech), rabbit anti-citrate synthase (1:1000, #16131, Proteintech), rabbit anti-DRP1 (1:1000, #12957, Proteintech), rabbit anti-MFF (1:1000, #17090, Proteintech), rabbit anti-FIS1 (1:1000, #10956, Proteintech), and anti-β-actin (1:5000, #20536, Proteintech) in TBS containing 0.1% BSA at 4 °C overnight. The membranes were then incubated with IRDye 800 CW goat-anti rabbit secondary antibodies (1:5000, #31460, Thermo Fisher Scientific) for 90 min at room temperature and visualized with an Odyssey scanner (Bio-Rad, California, USA). Quantification analysis of the blots was performed using NIH Image J software.

Statistical analyses

The normality of data and homogeneity of variance are tested by Shapiro-Wilk and Levene respectively. Single factor analysis of variance (one-way ANOVA) was used to compare the differences between groups. When the variance is homogeneous, the least significant difference (LSD) post-hoc test was used for multiple comparisons among groups. When the variance is not homogeneous, the Dunnett T3 method was used for comparison among groups. The differences are considered significant when $P < 0.05$. Data are expressed as means ± standard deviation (Mean ± SD). All statistical analyzes were conducted using SPSS 19.0.

Results

Changes in Harderian gland weight (HGW) and Harderian gland weight to carcass weight ratio (HGW/CW) in hamsters under different photoperiods

The HGW was significantly lower in SP (5%, $P < 0.05$) and LP (5%, $P < 0.05$) group than MP group, while the HGW/CW ratio demonstrated no significant differences among the three groups (Fig. 1).

INSERT FIGURE 1 HERE

Ultrastructural changes in HG nuclei, mitochondria, and autophagolysosomes

A large number of secretory cells were observed in the HGs of the three different photoperiod groups, including a large number of round- or elliptical-shaped fat droplets. The plasma membrane of the secretory cells was clearly visible. The mitochondria in the HG were irregularly oval, the cristae were clearly visible, and the membrane was complete. There was no significant difference in nuclear and mitochondrial

morphology among the three groups. Typical autophagolysosomal structures were observed in the LD group, showing a clear membrane structure on the outside and wrapped contents in the middle. In other groups, however, it was difficult to observe typical autophagolysosomal structures (Fig. 2).

INSERT FIGURE 2 HERE

DNA fragmentation

TUNEL staining provided direct evidence of apoptosis. In three photoperiodic groups, random HG sections showed that DNA fragmentation (represented by green fluorescence) were observed (Fig. 3).

INSERT FIGURE 3 HERE

Changes in LC3 and P62 puncta in HG under different photoperiods

The number of cytoplasmic LC3 puncta per 1 000 μm^2 is indicative of LC3I to LC3II conversion. Representative figures of LC3 immunofluorescence staining are shown in Fig. 4a, which significantly higher 77% and 172% ($P < 0.05$) in the SP and LP group, respectively, than that in the MP group (Fig. 4b).

Representative figures of P62 immunofluorescence staining are shown in Fig. 4a The number of P62 puncta was lowest in the LP group, with 43% ($P < 0.05$) less P62 puncta in the MP group (Fig. 4c).

INSERT FIGURE 4 HERE

Relative protein expression of apoptosis related factors

The contents of bax, bcl2, and Cyto C were detected by Western blot analysis, as shown in Figure 5a. The ratio of bax/bcl2 and the protein expression of Cyto C all showed no significant difference between three groups (Fig. 5b).

INSERT FIGURE 5 HERE

Relative protein expression of autophagy related factors

The contents of LC3 and P62 were detected by Western blot analysis, as shown in Figure 6a. The LC3II/LC3I level showed higher in SP (43%, $P < 0.05$) and LP groups (113%, $P < 0.05$) than that in MP group. Meanwhile, the protein expression of P62 showed LP group was lower ($P < 0.05$) than SP and MP groups (Fig. 6b).

INSERT FIGURE 6 HERE

Relative protein expression of mitochondrial related factors

The contents of ATP synthase, CS, DRP1, MFF, and FIS1 were detected by Western blot analysis, as shown in Figure 7a. CS, DRP1, and FIS1 protein expression showed no significant differences among the three groups. ATP synthase and MFF protein expression in the MD group was significantly increased ($P < 0.05$) compared with that in the other two groups (Fig. 7b).

INSERT FIGURE 7 HERE

Discussion

Our results showed that, compared with the moderate photoperiod control group, the HG weight of hamsters was significantly reduced under short and long photoperiods. The protein expression levels of bax/bcl2 and Cyto C also showed no significant differences among groups. In contrast, the protein expression of LC3II/LC3I was higher in the short and long photoperiod groups compared with the moderate photoperiod control. Furthermore, protein expression of ATP synthase and MFF was highest in the moderate photoperiod control group.

We found that after 10 weeks of different light treatment, HG weight in the short and long photoperiod groups was lower than that in the moderate photoperiod group. However, the HG weight to carcass weight ratio in the short and long photoperiod groups was slight change, suggesting that the decrease in HG weight may be consistent with a change in animal carcass weight.

To explore the mechanism of the above phenomenon, we studied the apoptosis level in HG of hamsters under different photoperiods and found that DNA fragmentation occurred in all three groups and ultrastructure analysis also showed that there was no significant nuclear change in the secretory cells of the HG during three groups. The bax/bcl2 ratio is often used to measure the degree of cell apoptosis and Cyto C is the key signal of apoptosis. (13, 14). Our study showed that although bax decreased significantly in the long photoperiod group, the ratio of bax to bcl2 and the protein expression of Cyto C remained stable, indicating that the level of apoptosis might be stable among the three groups. High-intensity light stimulation or high-dose MT injection can lead to increased cell necrosis in the HG of female Syrian hamsters and male rats (15). Since melatonin is usually positively correlated with the time to enter darkness (3, 16, 17), this may mean that short photoperiod exposure may increase the apoptosis level in HG. However, our research did not find this. On the one hand, it may be that exogenous injection of MT is not the same as simple photoperiod treatment. On the other hand, Syrian hamsters hibernate in winter (44), whereas striped dwarf hamsters display daily torpor (45). Therefore, the effects on these two hamsters differ under the short photoperiod of winter.

Interestingly, we found that the protein expression of LC3II/LC3I was higher in the short and long photoperiod groups than that in the moderate photoperiod control. As LC3II is a key protein of autophagolysosome membrane formation (20, 21), this result indicates that the level of autophagy may be higher in these two groups. In addition, the number of cytoplasmic LC3 puncta, which is indicative of LC3I to LC3II conversion, showed the same trend as LC3II/LC3I protein expression, which also suggests an increase in autophagy level. P62 is an autophagic transport protein, the accumulation of which indicates a decrease in autophagic efficiency (24). Here, immunofluorescence histochemistry showed that P62 protein aggregates and expression levels were lower in the long photoperiod group than in the other two groups, indicating that the level of autophagy might be highest under long photoperiod conditions. This is consistent with the ultrastructural results, showing the occurrence of autolysosomes. As the balance between apoptosis and autophagy is an important mechanism for tissue weight

maintenance (7), the higher autophagy level under the short and long photoperiods compared to the moderate photoperiod may be the main reason for the lower HG weight in hamsters.

We also found that ATP synthase protein expression levels were lower following short and long photoperiod treatment, consistent with the change in mitochondrial fission level. CS is a rate-limiting enzyme in the tricarboxylic acid cycle and represents the ability of mitochondria to undertake aerobic oxidation (28, 29). ATP synthase is the last step in ATP production by mitochondria, representing the ability of mitochondria to supply energy (30). In this study, the protein expression levels of ATP synthase in the HG were lower under short and long photoperiod conditions, whereas CS was maintained, indicating that the mitochondrial energy supply function was weakened slightly, and mitochondrial aerobic capacity remained unchanged. As ultrastructural analysis showed that mitochondria remained relatively intact in the three groups, we speculated that mitochondrial function may not have been weakened significantly. Drp1 is a key factor related to the promotion of mitochondrial fission, with MFF and FIS1 found to up- and down-regulate DRP1 activity, respectively (33, 35). In the short and long photoperiod groups, MFF protein expression decreased, whereas that of DRP1 and FIS1 remained unchanged. Considering that MFF is the up-regulatory factor of mitochondrial fission, rather than the most important factor, these results indicate that the mitochondrial fission level may have decreased slightly, which could be one of the reasons for the slight decrease in mitochondrial energy supply.

In summary, this study extends novel findings on the effects of photoperiod on morphological and functional changes in the HG and related mechanisms under different photoperiods (Fig. 7). As there were no significant changes in the level of apoptosis in the HG under the different photoperiods, the significant up-regulation in autophagy level under long and short photoperiod conditions may be the main factor leading to tissue weight loss. Mitochondrial function weakened slightly under short and long photoperiod treatment, which may be caused by the maintenance of apoptosis and down-regulation of mitochondrial fission. Photoperiod treatment in the non-breeding season (i.e., short and long photoperiods) led to different levels of degeneration in the morphology and function of the HG in hamsters, with the possible mechanism involving autophagy and mitochondrial fission.

Acknowledgments

Not applicable.

Author Contributions

ZW, JX, and LX conceived and designed research; ZW, JX, JM, and XZ performed experiments; ZW analyzed data; ZW interpreted experimental results; ZW and JM prepared figures; ZW and JX drafted manuscript; MW and HX provided experimental guidance and suggestions for revision; JX, ZW, and LX edited manuscript and approved final version of manuscript.

Funding

This work was supported by funds from the National Natural Science Foundation of China (No. 31670385, 31570377, 31770455).

Availability of data and materials

The datasets used and/or analyzed during the current study are available from the corresponding author on reasonable request. Partial original images are included in the supplementary documents.

Ethics approval and consent to participate

All procedures followed the Laboratory Animal Guidelines for the Ethical Review of Animal Welfare (GB/T 35892-2018) and were approved by the Animal Care and Use Committee of Qufu Normal University (Permit Number: dwsc 2019010).

Consent for publication

Not applicable.

Competing interests

No conflicts of interest, financial or otherwise, are declared by the authors.

Legend of figures

Table 1 Effects of photoperiod on carcass weight (CW), Harderian gland wet weight (HGWW), and ratio of HGWW/CW in hamsters after 10 weeks

Group	SP	MP	LP
CW after photoperiod (g)	15.91±1.26	17.06±2.51	15.89±0.84
HGWW after photoperiod (mg)	22.5±1.83^{b}	25.1±1.57^{a}	22.9 ±1.5^{b}
HGWW/CW after photoperiod (mg/g)	1.42 ±0.12	1.47 ±0.07	1.44 ±0.07

Values are means ± SD. n = 10. SP, short photoperiod; MP, moderate photoperiod; LP, long photoperiod. Different letters identify statistically significant difference ($P < 0.05$).

Fig. 1 Ultrastructure of HG in hamsters from three photoperiodic groups

(a) Nucleus ultrastructure of HG in hamsters from three photoperiodic groups. There were no significant differents in nuclear (N) morphology among three photoperiodic groups. Large number of fat droplets (FD) were observed in secretory cells of HG. Scale bar = 2 μm. (b) Cristae of mitochondria of HG in hamsters from three photoperiodic groups. There were no significant differents in mitochondrial (#) morphology among three groups. Scale bar = 0.2 μm. (C) Autophagolysosomes of HG in hamsters from three photoperiodic groups. Significant autophagolysosomal structures (see arrow) were observed in LP group. In other groups, autophagolysosomal structures were hardly

observed. Scale bar = 0.2 μm. SP, short photoperiod; MP, moderate photoperiod; LP, long photoperiod.

Fig. 2 Fluorescent terminal deoxynucleotidyl transferase biotin-dUTP nick end labeling (TUNEL) staining of HG in hamsters in three photoperiodic groups

Immunofluorescence histochemistry showing cell apoptosis, cell boundaries, and nuclei. Blue represents 4'6'-diamidino-2-phenylindole (DAPI)-stained nucleus, red represents Alexa Fluor 647-stained laminin of interstitial tissue, green represents TUNEL by FITC. Scale bar = 50 μm. SP, short photoperiod; MP, moderate photoperiod; LP, long photoperiod.

Fig. 3 Quantification of LC3 and P62 puncta of HG in hamsters in three photoperiodic groups

(a) Immunofluorescence histochemistry showing LC3 and P62 puncta. green represents AF488-stained LC3 or P62, respectively. Scale bar = 50 μm. (b) Quantification of LC3 puncta. (c) Quantification of P62 puncta. Six figures were analyzed in each sample; ten samples were analyzed in each group. Values are means ± SD. SP, short photoperiod; MP, moderate photoperiod; LP, long photoperiod. Different letters identify statistically significant difference ($P < 0.05$).

Fig. 4 Changes in protein levels of apoptosis related factors in HG of hamsters in three different photoperiodic groups

(a) Representative immunoblots of bax, bcl2, Cyto C, and β-actin in three different photoperiodic groups. (b) Ratio of bax, bcl2, Cyto C to β-actin and ratio of bax to bcl2 in HG of hamsters in three different photoperiodic groups. Values are means ± SD. n=10. SP, short photoperiod; MP, moderate photoperiod; LP, long photoperiod. Different letters identify statistically significant difference ($P < 0.05$).

Fig. 5 Changes in protein levels of autophagy related factors in HG of hamsters in three different photoperiodic groups

(a) Representative immunoblots of LC3, P62, and β-actin in three different photoperiodic groups. (b) Ratio of LC3, P62 to β-actin in HG of hamsters in three different photoperiodic groups. Values are means ± SD. n=10. SP, short photoperiod; MP, moderate photoperiod; LP, long photoperiod. Different letters identify statistically significant difference ($P < 0.05$).

Fig. 6 Changes in protein levels of mitochondrial related factors in HG of hamsters in three different photoperiodic groups

(a) Representative immunoblots of ATP synthase, CS, DRP1, MFF, FIS1, and β-actin in three different photoperiodic groups. (b) Ratio of ATP synthase, CS, DRP1, MFF, FIS1 to β-actin in HG of hamsters in three different photoperiodic groups. Values are means ± SD. n = 10. SP, short photoperiod; MP, moderate photoperiod; LP, long

photoperiod. Different letters identify statistically significant difference ($P < 0.05$).

Fig. 7 Graphical summary of study

LC3, microtubule-associated protein 1 light chain; P62, sequestosome 1; Cyto C, cytochrome C; FIS1, fission 1; MFF, mitochondrial fission factor; DRP1, dynamin-related protein 1; ATP synthase, adenosine triphosphate synthase; CS, citrate synthase; SP, short photoperiod; LP, long photoperiod.

References

1. Nakayama T, Yoshimura T. Seasonal Rhythms: The Role of Thyrotropin and Thyroid Hormones. Thyroid : official journal of the American Thyroid Association. 2018;28(1):4-10.
2. Masson-Pevet M, Naimi F, Canguilhem B, Saboureau M, Bonn D, Pevet P. Are the annual reproductive and body weight rhythms in the male European hamster (Cricetus cricetus) dependent upon a photoperiodically entrained circannual clock? Journal of pineal research. 1994;17(4):151-63.
3. Buzzell GR. The Harderian gland: perspectives. Microscopy research and technique. 1996;34(1):2-5.
4. Sakai T. Major ocular glands (harderian gland and lacrimal gland) of the musk shrew (Suncus murinus) with a review on the comparative anatomy and histology of the mammalian lacrimal glands. Journal of morphology. 1989;201(1):39-57.
5. Dubey S, Haldar C. Environmental factors and annual harderian-pineal-gonadal interrelationship in Indian jungle bush quail, Perdicula asiatica. General and comparative endocrinology. 1997;106(1):17-22.
6. Borniger JC, Nelson RJ. Photoperiodic regulation of behavior: Peromyscus as a model system. Seminars in cell & developmental biology. 2017;61:82-91.
7. Gonzalez CR, Isla MLM, Vitullo AD. The balance between apoptosis and autophagy regulates testis regression and recrudescence in the seasonal-breeding South American plains vizcacha, Lagostomus maximus. Plos One. 2018;13(1).
8. Monteforte R, Santillo A, Lanni A, D'Aniello S, Baccari GC. Morphological and biochemical changes in the Harderian gland of hypothyroid rats. J Exp Biol. 2008;211(4):606-12.
9. Kurisu K, Sawamoto O, Watanabe H, Ito A. Sequential changes in the harderian gland of rats exposed to high intensity light. Laboratory animal science. 1996;46(1):71-6.
10. Fu WW, Hu HX, Dang K, Chang H, Du B, Wu X, et al. Remarkable preservation of Ca2+ homeostasis and inhibition of apoptosis contribute to anti-muscle atrophy effect in hibernating Daurian ground squirrels. Sci Rep-Uk. 2016;6:13.
11. Zha H, Aime-Sempe C, Sato T, Reed JC. Proapoptotic protein Bax heterodimerizes with Bcl-2 and homodimerizes with Bax via a novel domain (BH3) distinct from BH1 and BH2. The Journal of biological chemistry. 1996;271(13):7440-4.
12. Smith HK, Maxwell L, Martyn JA, Bass JJ. Nuclear DNA fragmentation and

456 morphological alterations in adult rabbit skeletal muscle after short-term
457 immobilization. Cell and tissue research. 2000;302(2):235-41.
458 13. Antonsson B, Conti F, Ciavatta A, Montessuit S, Lewis S, Martinou I, et al. Inhibition
459 of Bax channel-forming activity by Bcl-2. Science. 1997;277(5324):370-2.
460 14. Korsmeyer SJ, Shutter JR, Veis DJ, Merry DE, Oltvai ZN. Bcl-2/Bax: a rheostat that
461 regulates an anti-oxidant pathway and cell death. Seminars in cancer biology.
462 1993;4(6):327-32.
463 15. Vega-Naredo I, Caballero B, Sierra V, Garcia-Macia M, de Gonzalo-Calvo D, Oliveira
464 PJ, et al. Melatonin modulates autophagy through a redox-mediated action in female
465 Syrian hamster Harderian gland controlling cell types and gland activity. J Pineal Res.
466 2012;52(1):80-92.
467 16. Tsutsui K, Ubuka T. Photoperiodism in Mammalian Reproduction2018. 415-9 p.
468 17. Payne AP. The harderian gland: a tercentennial review. Journal of anatomy.
469 1994;185 (Pt 1):1-49.
470 18. Biazik J, Vihinen H, Anwar T, Jokitalo E, Eskelinen EL. The versatile electron
471 microscope: an ultrastructural overview of autophagy. Methods (San Diego, Calif).
472 2015;75:44-53.
473 19. Dong S, Zhao S, Wang Y, Pang T, Ru Y. [Analysis of blood cell autophagy distribution
474 in hematologic diseases by transmission electron microscope]. Zhonghua xue ye xue
475 za zhi = Zhonghua xueyexue zazhi. 2015;36(2):144-7.
476 20. Lee YK, Lee JA. Role of the mammalian ATG8/LC3 family in autophagy: differential
477 and compensatory roles in the spatiotemporal regulation of autophagy. BMB reports.
478 2016;49(8):424-30.
479 21. Schaaf MB, Keulers TG, Vooijs MA, Rouschop KM. LC3/GABARAP family proteins:
480 autophagy-(un)related functions. FASEB journal : official publication of the Federation
481 of American Societies for Experimental Biology. 2016;30(12):3961-78.
482 22. Mizushima N, Yoshimori T. How to interpret LC3 immunoblotting. Autophagy.
483 2007;3(6):542-5.
484 23. Zhang YB, Gong JL, Xing TY, Zheng SP, Ding W. Autophagy protein p62/SQSTM1 is
485 involved in HAMLET-induced cell death by modulating apotosis in U87MG cells. Cell
486 Death Dis. 2013;4.
487 24. Lamark T, Svenning S, Johansen T. Regulation of selective autophagy: the
488 p62/SQSTM1 paradigm. Essays in biochemistry. 2017;61(6):609-24.
489 25. Kongsuphol P, Mukda S, Nopparat C, Villarroel A, Govitrapong P. Melatonin
490 attenuates methamphetamine-induced deactivation of the mammalian target of
491 rapamycin signaling to induce autophagy in SK-N-SH cells. J Pineal Res. 2009;46(2):199-
492 206.
493 26. Nopparat C, Porter JE, Ebadi M, Govitrapong P. The mechanism for the
494 neuroprotective effect of melatonin against methamphetamine-induced autophagy. J
495 Pineal Res. 2010;49(4):382-9.
496 27. Coto-Montes A, Tomas-Zapico C. Could melatonin unbalance the equilibrium
497 between autophagy and invasive processes? Autophagy. 2006;2(2):126-8.

28. Wiegand G, Remington SJ. Citrate synthase: structure, control, and mechanism. Annual review of biophysics and biophysical chemistry. 1986;15:97-117.
29. Remington SJ. Structure and mechanism of citrate synthase. Current topics in cellular regulation. 1992;33:209-29.
30. Kramarova TV, Shabalina IG, Andersson U, Westerberg R, Carlberg I, Houstek J, et al. Mitochondrial ATP synthase levels in brown adipose tissue are governed by the c-Fo subunit P1 isoform. Faseb Journal. 2008;22(1):55-63.
31. Kraus F, Ryan MT. The constriction and scission machineries involved in mitochondrial fission. Journal of cell science. 2017;130(18):2953-60.
32. Tilokani L, Nagashima S, Paupe V, Prudent J. Mitochondrial dynamics: overview of molecular mechanisms. Essays in biochemistry. 2018;62(3):341-60.
33. Tieu Q, Nunnari J. Mdv1p is a WD repeat protein that interacts with the dynamin-related GTPase, Dnm1p, to trigger mitochondrial division. The Journal of cell biology. 2000;151(2):353-66.
34. Liu R, Chan DC. The mitochondrial fission receptor Mff selectively recruits oligomerized Drp1. Molecular biology of the cell. 2015;26(24):4466-77.
35. Yu R, Jin SB, Lendahl U, Nister M, Zhao J. Human Fis1 regulates mitochondrial dynamics through inhibition of the fusion machinery. EMBO J. 2019;38(8).
36. Vaughan MK, Menendez-Pelaez A, Buzzell GR, Vaughan GM, Little JC, Reiter RJ. Circadian rhythms in reproductive and thyroid hormones in gonadally regressed male hamsters exposed to natural autumn photoperiod and temperature conditions. Neuroendocrinology. 1994;60(1):96-104.
37. Menendez-Pelaez A, Lopez-Gonzalez MA, Guerrero JM. Melatonin binding sites in the Harderian gland of Syrian hamsters: sexual differences and effect of castration. J Pineal Res. 1993;14(1):34-8.
38. Buzzell GR, Blank JL, Vaughan MK, Reiter RJ. Control of secretory lipid droplets in the harderian gland by testosterone and the photoperiod: comparison of two species of hamsters. General and comparative endocrinology. 1995;99(2):230-8.
39. Xu LX, Xue HL, Li SN, Xu JH, Chen L. Seasonal differential expression of KiSS-1/GPR54 in the striped hamsters (Cricetulus barabensis) among different tissues. Integr Zool. 2017;12(3):260-8.
40. Xue HL, Xu JH, Chen L, Xu LX. Genetic variation of the striped hamster (Cricetulus barabensis) and the impact of population density and environmental factors. Zool Stud. 2014;53:8.
41. Zhao L, Zhong M, Xue HL, Ding JS, Wang S, Xu JH, et al. Effect of RFRP-3 on reproduction is sex- and developmental status-dependent in the striped hamster (Cricetulus barabensis). Gene. 2014;547(2):273-9.
42. Wang Z, Jiang SF, Cao J, Liu K, Xu SH, Arfat Y, et al. Novel findings on ultrastructural protection of skeletal muscle fibers during hibernation of Daurian ground squirrels: Mitochondria, nuclei, cytoskeleton, glycogen. J Cell Physiol. 2019.
43. Wang Z, Jiang SF, Cao J, Liu K, Xu SH, Arfat Y, et al. Novel findings on ultrastructural protection of skeletal muscle fibers during hibernation of Daurian ground squirrels:

Mitochondria, nuclei, cytoskeleton, glycogen. J Cell Physiol. 2019;234(8):13318-31.
44. Sato T, Tachiwana T, Takata K, Tay TW, Ishii M, Nakamura R, et al. Testicular dynamics in Syrian hamsters exposed to both short photoperiod and low ambient temperature. Anatomia Histologia Embryologia. 2005;34(4):220-4.
45. Ushakova MV, Kropotkina MV, Feoktistova NY, Surov AV. Daily Torpor in Hamsters (Rodentia, Cricetinae). Russ J Ecol. 2012;43(1):62-6.

Figures

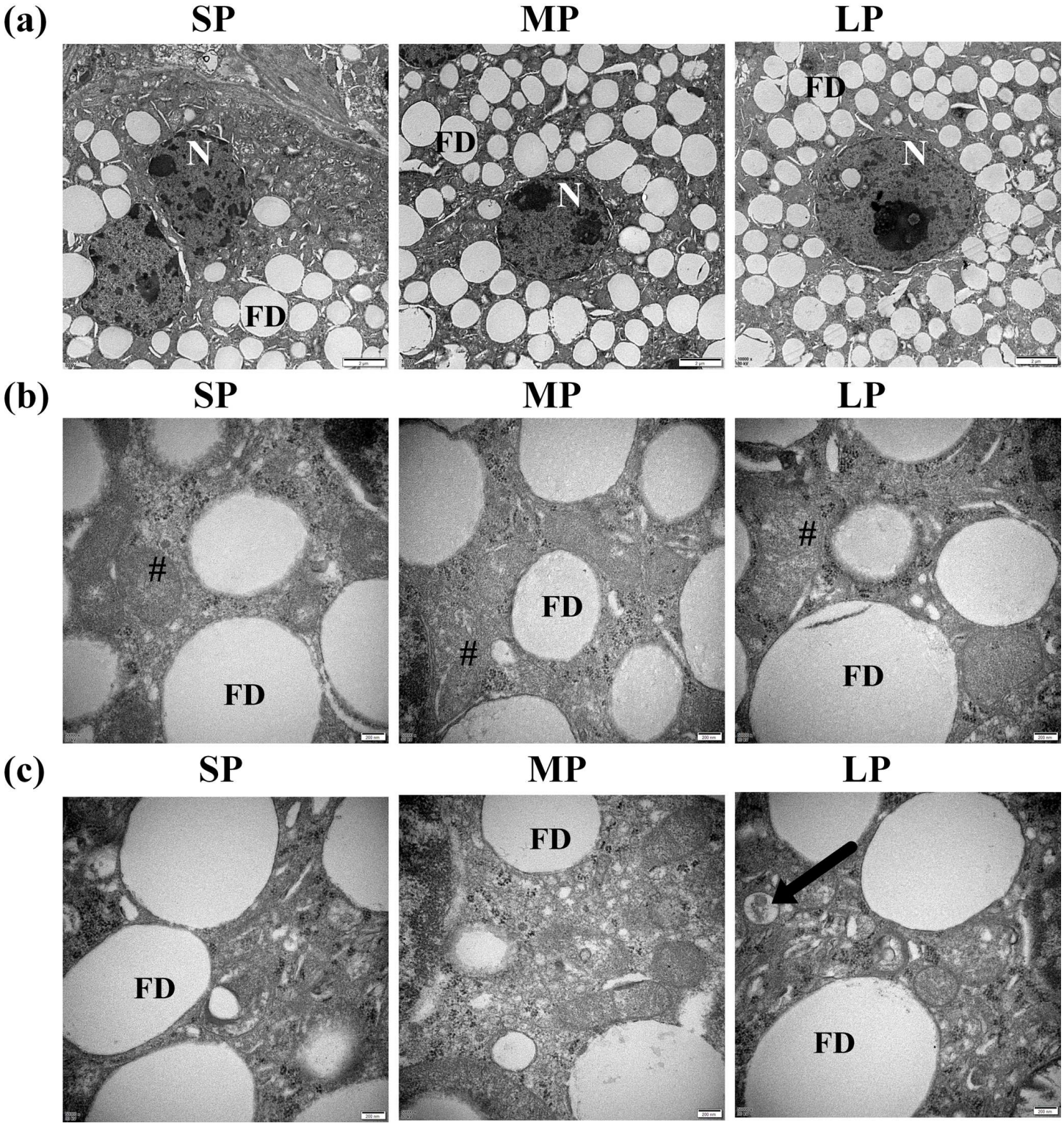

Figure 1

Ultrastructure of HG in hamsters from three photoperiodic groups. (a) Nucleus ultrastructure of HG in hamsters from three photoperiodic groups. There were no significant differents in nuclear (N) morphology among three photoperiodic groups. Large number of fat droplets (FD) were observed in secretory cells of

HG. Scale bar = 2 μm. (b) Cristae of mitochondria of HG in hamsters from three photoperiodic groups. There were no significant differents in mitochondrial (#) morphology among three groups. Scale bar = 0.2 μm. (C) Autophagolysosomes of HG in hamsters from three photoperiodic groups. Significant autophagolysosomal structures (see arrow) were observed in LP group. In other groups, autophagolysosomal structures were hardly observed. Scale bar = 0.2 μm. SP, short photoperiod; MP, moderate photoperiod; LP, long photoperiod.

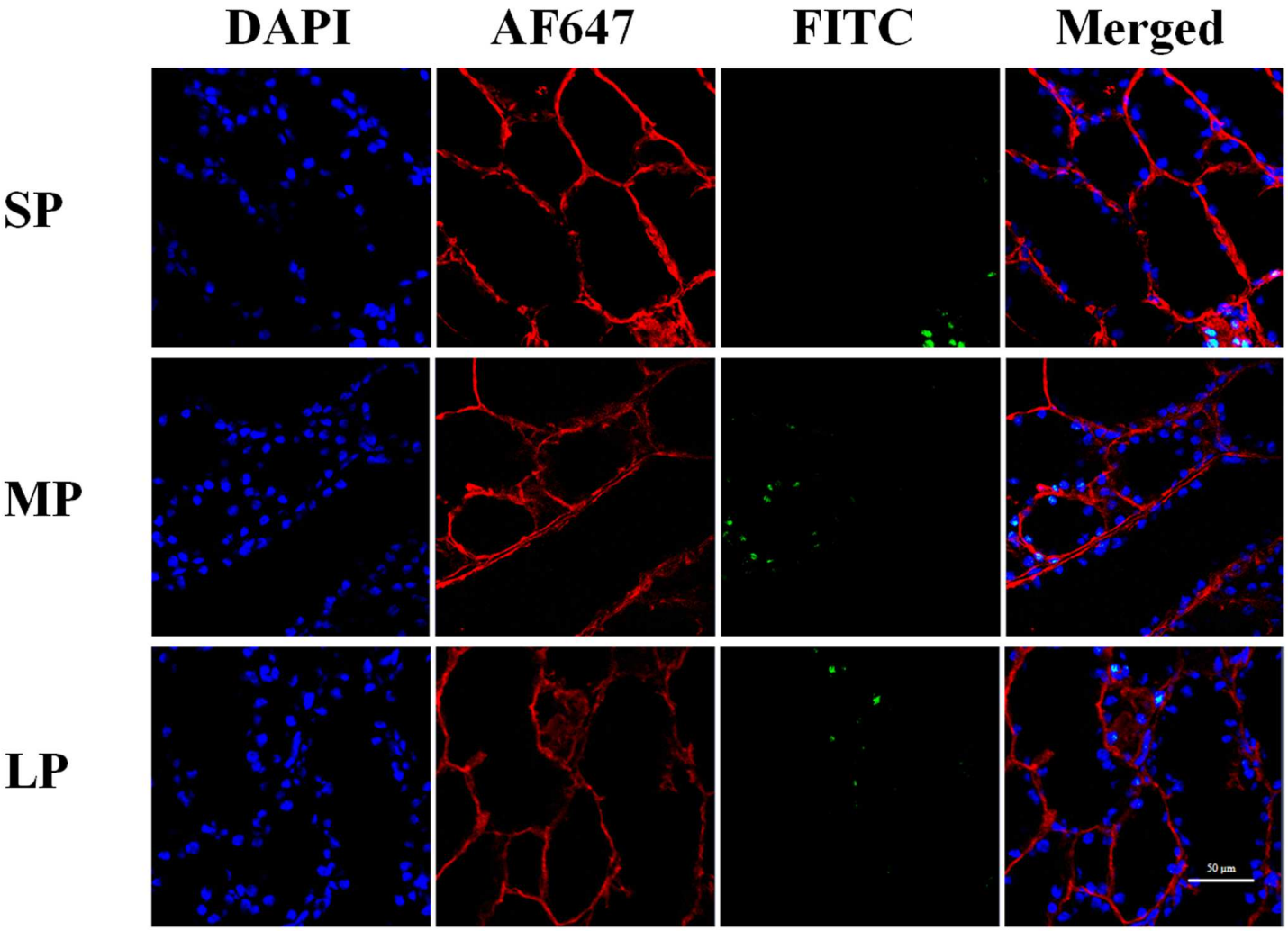

Figure 2

Fluorescent terminal deoxynucleotidyl transferase biotin-dUTP nick end labeling (TUNEL) staining of HG in hamsters in three photoperiodic groups. Immunofluorescence histochemistry showing cell apoptosis, cell boundaries, and nuclei. Blue represents 4’6’-diamidino-2-phenylindole (DAPI)-stained nucleus, red represents Alexa Fluor 647-stained laminin of interstitial tissue, green represents TUNEL by FITC. Scale bar = 50 μm. SP, short photoperiod; MP, moderate photoperiod; LP, long photoperiod.

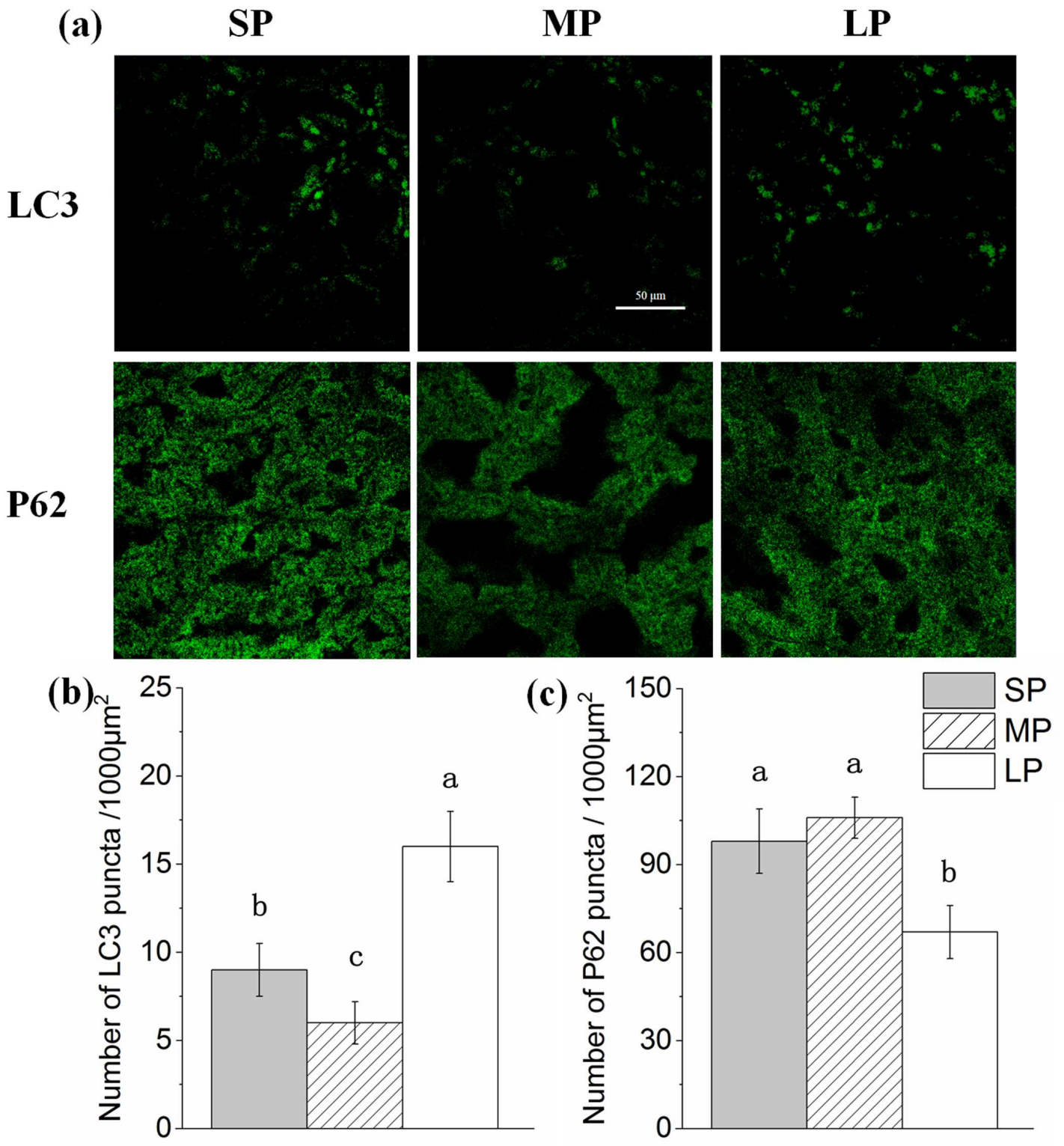

Figure 3

Quantification of LC3 and P62 puncta of HG in hamsters in three photoperiodic groups. (a) Immunofluorescence histochemistry showing LC3 and P62 puncta. green represents AF488-stained LC3 or P62, respectively. Scale bar = 50 μm. (b) Quantification of LC3 puncta. (c) Quantification of P62 puncta. Six figures were analyzed in each sample; ten samples were analyzed in each group. Values are

means ± SD. SP, short photoperiod; MP, moderate photoperiod; LP, long photoperiod. Different letters identify statistically significant difference ($P < 0.05$).

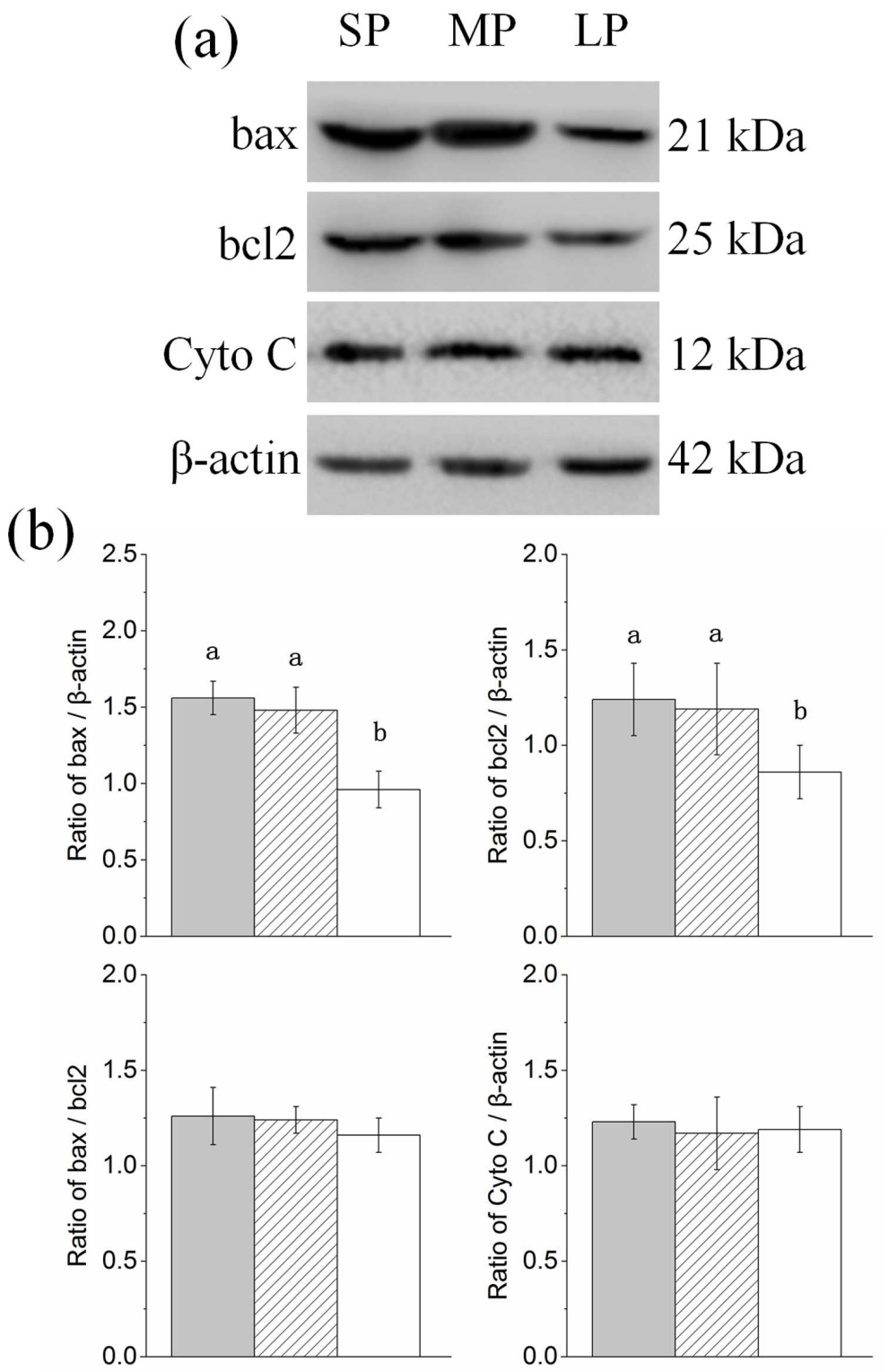

Figure 4

Changes in protein levels of apoptosis related factors in HG of hamsters in three different photoperiodic groups. (a) Representative immunoblots of bax, bcl2, Cyto C, and β-actin in three different photoperiodic groups. (b) Ratio of bax, bcl2, Cyto C to β-actin and ratio of bax to bcl2 in HG of hamsters in three

different photoperiodic groups. Values are means ± SD. n=10. SP, short photoperiod; MP, moderate photoperiod; LP, long photoperiod. Different letters identify statistically significant difference ($P < 0.05$).

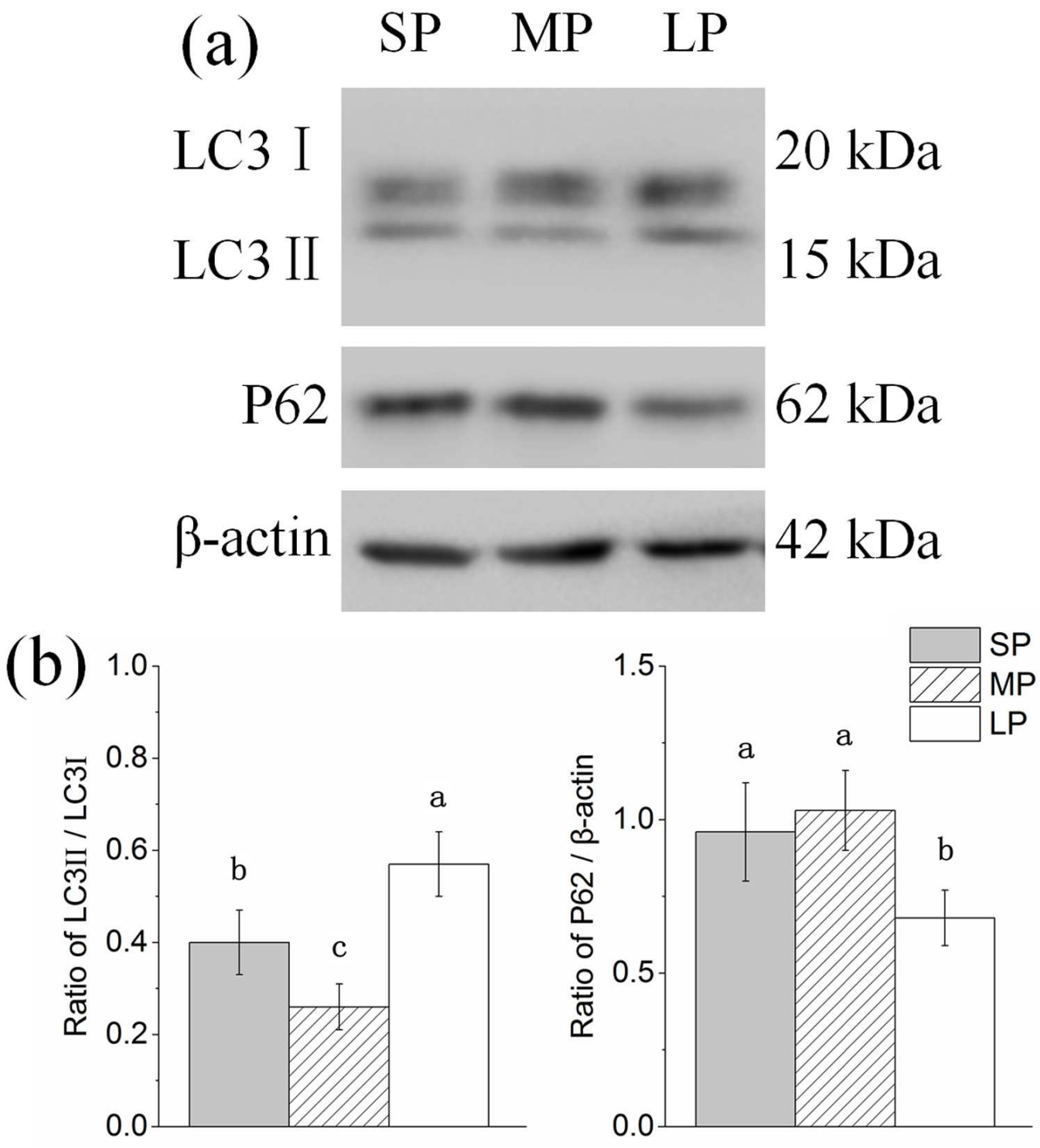

Figure 5

Changes in protein levels of autophagy related factors in HG of hamsters in three different photoperiodic groups. (a) Representative immunoblots of LC3, P62, and β-actin in three different photoperiodic groups. (b) Ratio of LC3, P62 to β-actin in HG of hamsters in three different photoperiodic groups. Values are

means ± SD. n=10. SP, short photoperiod; MP, moderate photoperiod; LP, long photoperiod. Different letters identify statistically significant difference ($P < 0.05$).

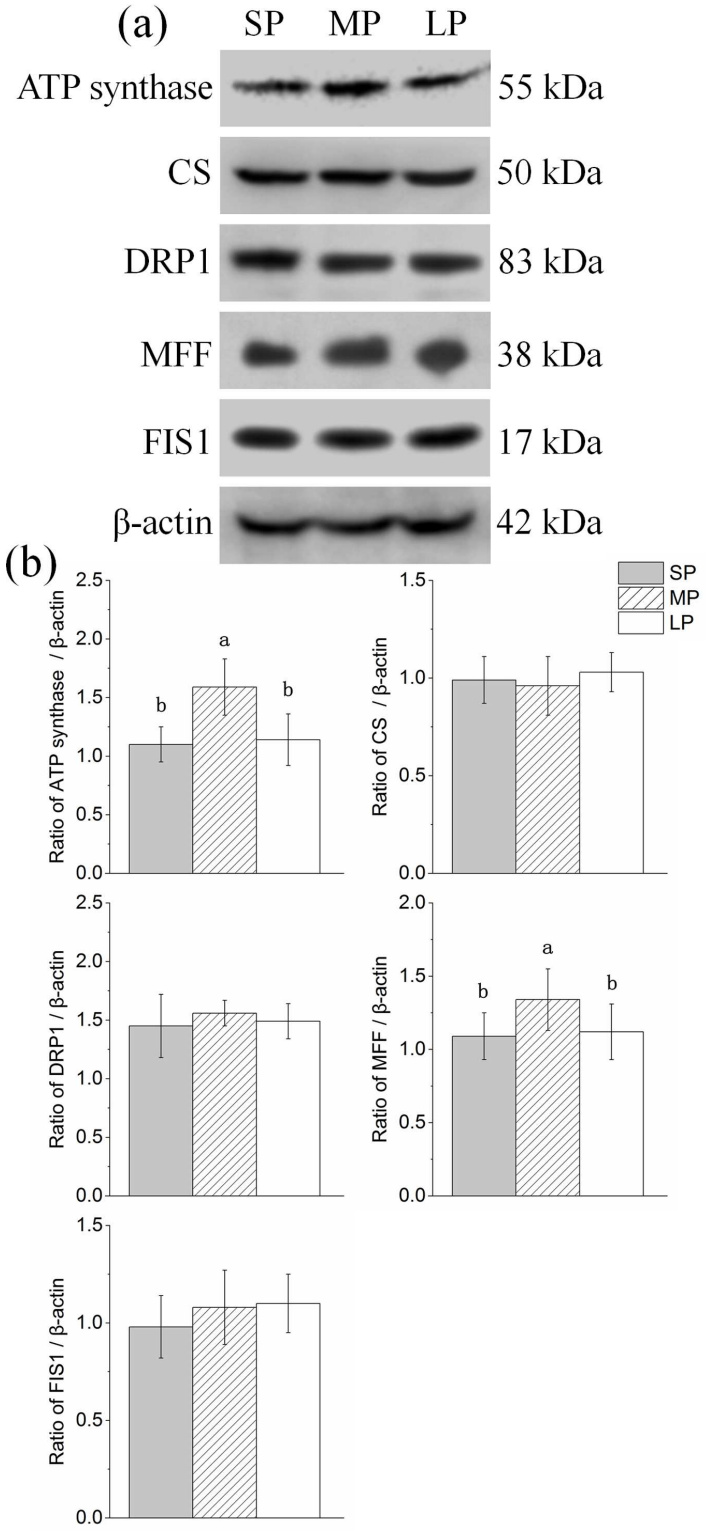

Figure 6

Changes in protein levels of mitochondrial related factors in HG of hamsters in three different photoperiodic groups. (a) Representative immunoblots of ATP synthase, CS, DRP1, MFF, FIS1, and β-actin in three different photoperiodic groups. (b) Ratio of ATP synthase, CS, DRP1, MFF, FIS1 to β-actin in HG of

hamsters in three different photoperiodic groups. Values are means ± SD. n = 10. SP, short photoperiod; MP, moderate photoperiod; LP, long photoperiod. Different letters identify statistically significant difference ($P < 0.05$).

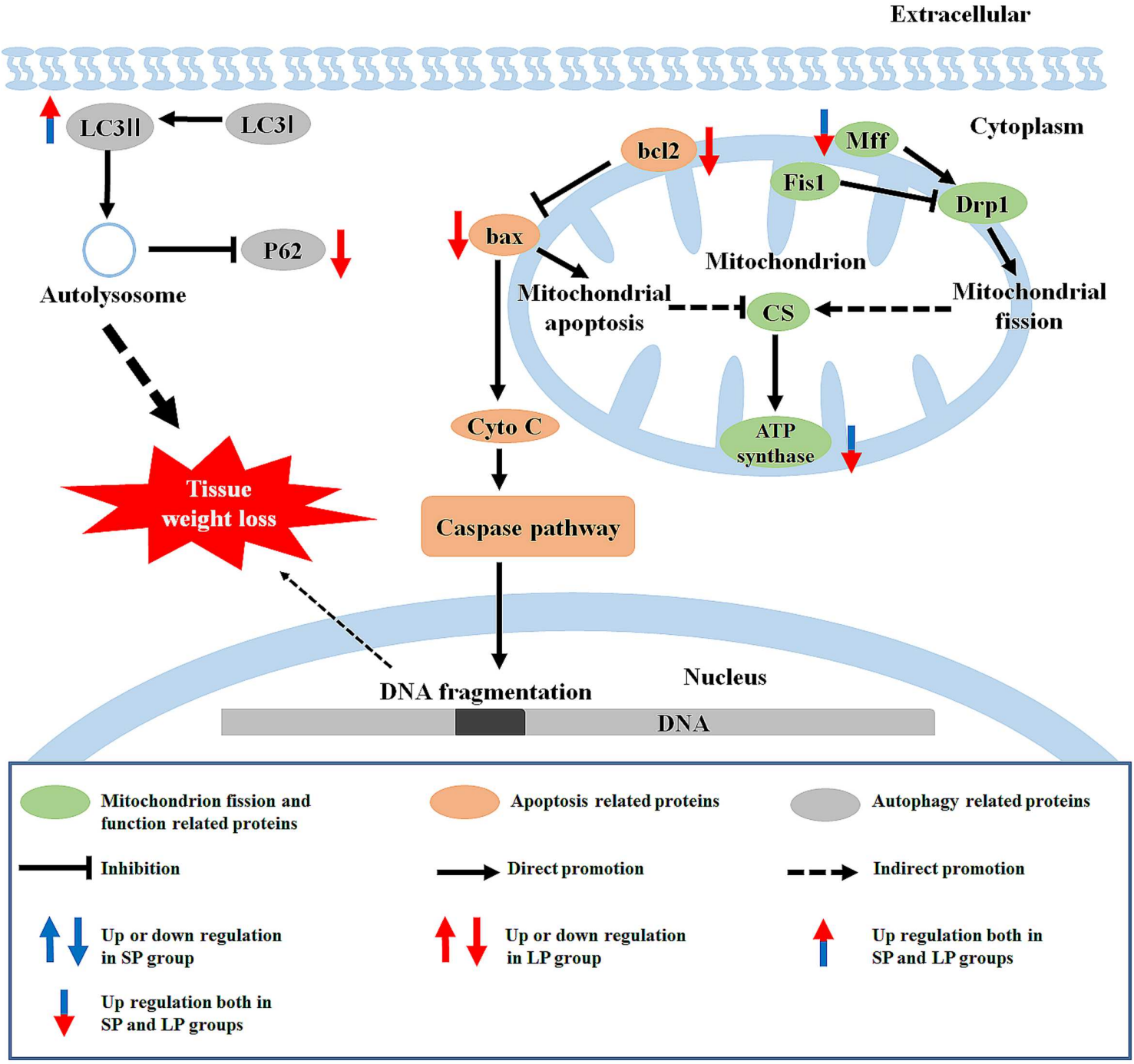

Figure 7

Graphical summary of study. LC3, microtubule-associated protein 1 light chain; P62, sequestosome 1; Cyto C, cytochrome C; FIS1, fission 1; MFF, mitochondrial fission factor; DRP1, dynamin- related protein 1; ATP synthase, adenosine triphosphate synthase; CS, citrate synthase; SP, short photoperiod; LP, long photoperiod.

Supplementary Files

This is a list of supplementary files associated with this preprint. Click to download.

- Supplementarydocument1.docx